QCD AND JETS

F. Hautmann

Theoretical Physics, University of Oxford, Oxford OX1 3PU, UK

(Received April 5, 2013)

We address aspects of jet physics at the Large Hadron Collider, focusing on features of recent jet measurements which challenge the theory. We discuss examples illustrating the role of QCD parton showers, nonperturbative corrections, soft multi-gluon emission.

DOI:10.5506/APhysPolB.44.761
PACS numbers: 12.38.–t

1. Introduction

The first three years of running of the LHC have probed jet physics in new ways, investigating previously unexplored kinematic regions. While next-to-leading-order (NLO) QCD calculations, supplemented with nonperturbative corrections and parton showers, are able to describe well inclusive jet spectra over a wide range of transverse momenta extending from 20 GeV to 2 TeV, several features of LHC jet data challenge the theory. This applies, in particular, to the behavior of cross sections with increasing rapidity; to correlations of multiple jets in rapidity, azimuthal angle, transverse energy; to non-inclusive observables probing the structure of high multiplicity final states.

This article focuses on aspects of jet production which, despite the presence of a high transverse momentum scale, are sensitive to soft gluon processes and QCD infrared physics. We start with inclusive cross sections in Sec. 2 and discuss the role of parton showering and nonperturbative effects in the context of matched NLO-shower event generators. In Sec. 3, we consider forward jets and examples of multi-jet correlations. Section 4 examines b-flavor jets. Section 5 takes a further look at jet correlations from the viewpoint of multiple parton interactions, emphasizing the role of energy flow variables. Section 6 addresses motivation and prospects for extending jet measurements to lower transverse momenta than is presently done.

2. Inclusive jet production

Measurements of inclusive jet production are carried out at the LHC [1, 2] over a kinematic range in transverse momentum and rapidity much larger than in any previous collider experiment [3]. Baseline comparisons with Standard Model theoretical predictions are based either on next-to-leading-order (NLO) QCD calculations, supplemented with nonperturbative (NP) corrections [1, 2] estimated from Monte Carlo event generators, or on NLO-matched parton shower event generators [4, 5]. The upper panels in Fig. 1 [1] report the first kind of comparison, showing that the NLO calculation agrees with data at central rapidities, while increasing deviations are seen with in-

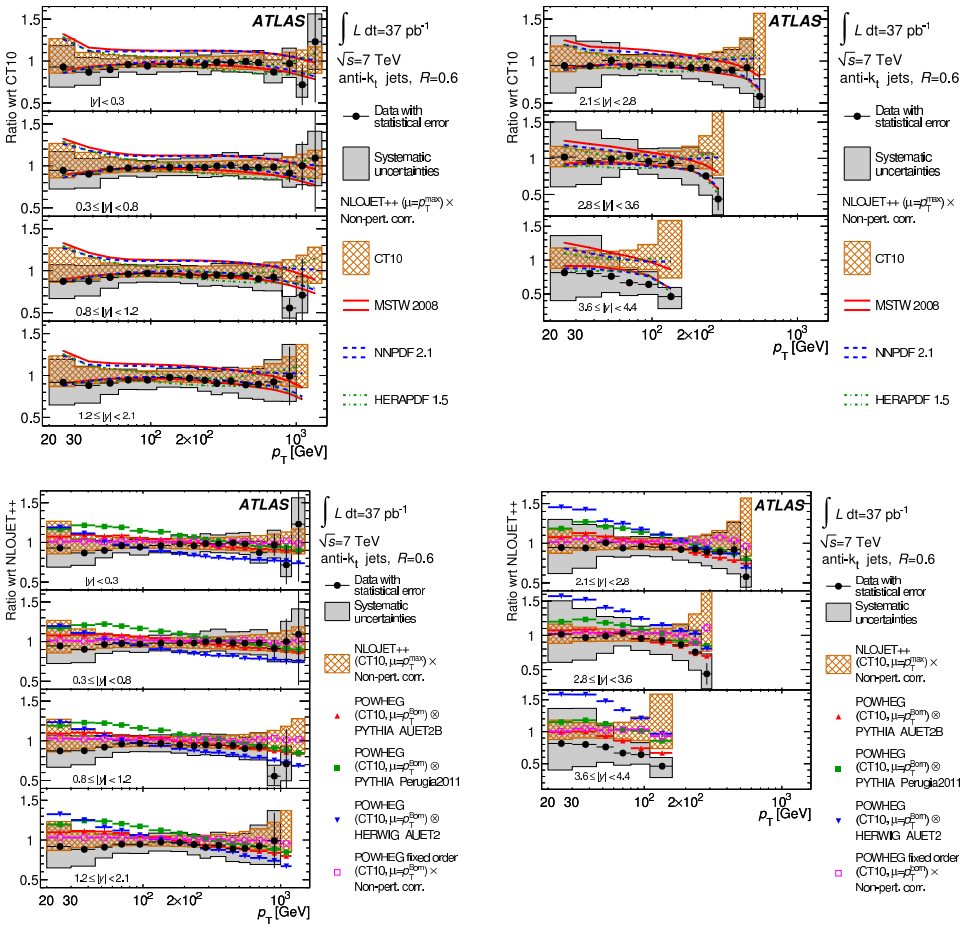

Fig. 1. Inclusive jet spectra [1] compared with (top) NLO+NP results and (bottom) NLO-matched shower results.

creasing rapidity at large transverse momentum p_{T} [1]. The question arises of whether such behavior is associated with higher-order perturbative contributions or with nonperturbative components of the cross section.

The lower panels in Fig. 1 [1] show the second kind of comparison based on POWHEG calculations [6], in which NLO matrix elements are matched with parton showers [7, 8]. This improves the description of data, indicating that higher-order radiative contributions taken into account via parton showers are numerically important. At the same time, the results show large differences between POWHEG calculations interfaced with different shower generators, HERWIG [7] and PYTHIA [8], in the forward rapidity region. This region is sensitive to the details of parton showering corrections.

It thus becomes apparent that the treatment of nonperturbative and showering contributions is essential for the understanding of LHC jet data. We discuss these in more detail next.

2.1. Nonperturbative and showering corrections

Using leading-order Monte Carlo (LO-MC) generators [7, 8], the nonperturbative correction factors are schematically obtained in [1, 2] as

$$K_0^{\mathrm{NP}} = N_{\mathrm{LO-MC}}^{(\mathrm{ps+mpi+had})} / N_{\mathrm{LO-MC}}^{(\mathrm{ps})}\,, \tag{1}$$

where (ps+mpi+had) and (ps) mean respectively a simulation including parton showers, multiparton interactions and hadronization, and a simulation including only parton showers in addition to the LO hard process.

While this is a natural way to estimate NP corrections from LO+PS event generators, it is noted in [9] that when these corrections are combined with NLO parton-level results a potential inconsistency arises because the radiative correction from the first gluon emission is treated at different levels of accuracy in the two parts of the calculation. To avoid this, Ref. [9] proposes a method to use NLO Monte Carlo (NLO-MC) generators to determine the correction. In this case, one can consistently assign correction factors to be applied to NLO calculations. Moreover, this method allows one to study separately correction factors to the fixed-order calculation due to parton showering effects. To this end, Ref. [9] introduces the correction factors K^{NP} and K^{PS} as

$$K^{\mathrm{NP}} = N_{\mathrm{NLO-MC}}^{(\mathrm{ps+mpi+had})} \Big/ N_{\mathrm{NLO-MC}}^{(\mathrm{ps})}\,, \tag{2}$$

$$K^{\mathrm{PS}} = N_{\mathrm{NLO-MC}}^{(\mathrm{ps})} \Big/ N_{\mathrm{NLO-MC}}^{(0)}\,, \tag{3}$$

where the denominator in Eq. (3) is defined by switching off all components beyond NLO in the Monte Carlo simulation.

The factor K^{NP} in Eq. (2) differs from K_0^{NP} because of the different definition of the hard process. In particular, the multi-parton interaction p_{T} cut-off scale is different in the LO and NLO cases. Numerical results are shown in Fig. 2. The factor K^{PS} in Eq. (3), on the other hand, is new. It singles out contributions due to parton showering and has not been considered in previous analyses. Unlike the NP correction, it gives finite effects also at large p_{T}. Results are given in Fig. 3, showing that this correction is not just a rescaling factor, but it is y and p_{T} dependent, especially when rapidity is non-central.

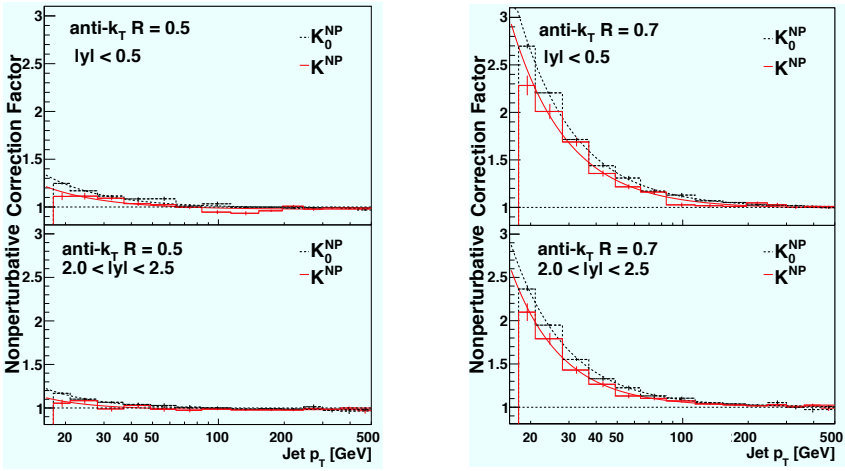

Fig. 2. The NP correction factors to jet transverse momentum distributions obtained from Eq. (1) and Eq. (2), using PYTHIA and POWHEG respectively, for $|y| < 0.5$ and $2 < |y| < 2.5$. Left: $R = 0.5$; right: $R = 0.7$ [9].

The correction factor in Fig. 3 comes from initial-state and final-state showers, and as noted in [9] these are so interrelated that the combined effect is nontrivial and cannot be obtained by simply adding the two. In general, the effect from parton shower is largest at large $|y|$, where the initial state parton shower is mainly contributing at low p_{T}, while the final state parton shower is contributing significantly over the whole p_{T} range. It is observed in [9] that the main initial state showering effect comes from kinematical shifts in longitudinal momentum distributions [10], due to combining collinearity approximations with the Monte Carlo implementation of energy-momentum conservation constraints. The effect of the kinematic shifts is illustrated in Fig. 4 [9], showing the distribution in the parton longitudinal momentum fraction x before parton showering and after parton showering. We see that the longitudinal shift is negligible for central rapidities but becomes significant for $y > 1.5$.

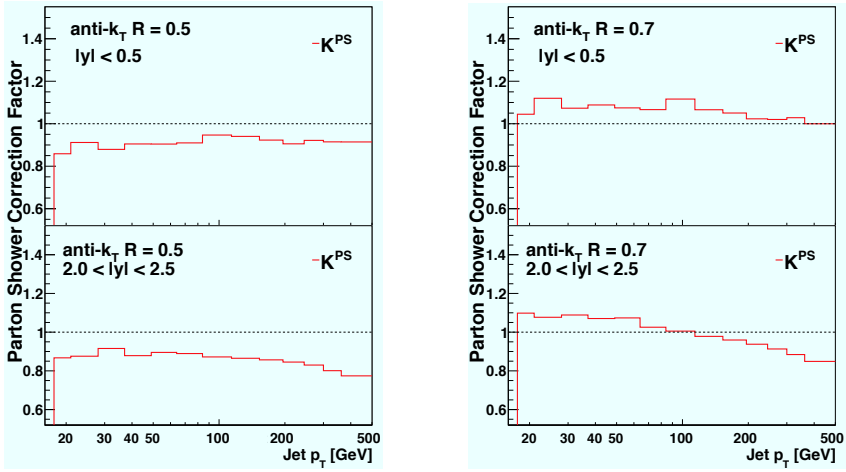

Fig. 3. The parton shower correction factor to jet transverse momentum distributions, obtained from Eq. (3) using POWHEG for $|y| < 0.5$ and $2 < |y| < 2.5$. Left: $R = 0.5$; right: $R = 0.7$ [9].

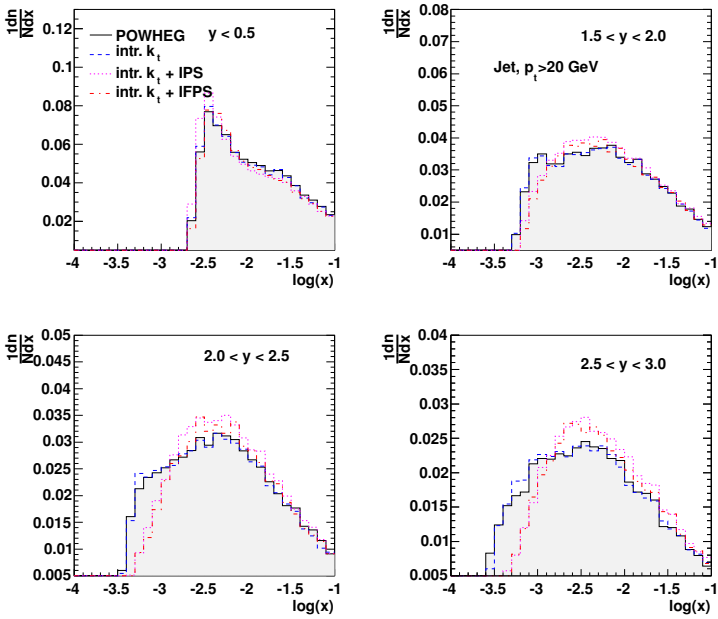

Fig. 4. Distributions in the parton longitudinal momentum fraction x before (POWHEG) and after parton showering (POWHEG+PS), for inclusive jet production at different rapidities for jets with $p_{\mathrm{T}} > 18$ GeV obtained by the anti-k_{t} jet algorithm [11] with $R = 0.5$. Shown is the effect of intrinsic k_{t}, initial (IPS) and initial+final state (IFPS) parton shower [9].

In summary, the nonperturbative correction factor $K^{\rm NP}$ introduced from NLO-MC in Eq. (2) gives non-negligible differences at low to intermediate jet $p_{\rm T}$, while the showering correction factor $K^{\rm PS}$ of Eq. (3) gives significant effects over the whole $p_{\rm T}$ range and is largest at large jet rapidities y. Because of this y and $p_{\rm T}$ dependence, taking properly into account NP and showering correction factors changes the shape of jet distributions, and may thus influence the comparison of theory predictions with experimental data. We anticipate, in particular, that taking account of the showering correction factor will be relevant in fits for parton distribution functions using inclusive jet data.

3. Forward jets

Physics in the forward region at hadron colliders is traditionally dominated by soft particle production. At the LHC, forward physics turns into a largely new field [12–14] because, due to the phase space opening up at large center-of-mass energies, both soft and hard production processes become relevant and, thanks to the unprecedented reach in rapidity of the experimental instrumentation, it becomes possible, for the first time at hadron–hadron colliders, to carry out a program of jet physics in the forward region. Forward jets enter the LHC physics program in an essential way both for new particle discovery processes (*e.g.*, Higgs searches in vector boson fusion channels, jet studies in decays of highly boosted heavy states) and new aspects of standard model physics (*e.g.*, QCD at small x and its interplay with cosmic ray physics, searches for new states of strongly interacting matter at high density).

We have discussed in the previous section that nonperturbative and showering corrections become especially pronounced for high rapidity, and so do kinematic effects due to longitudinal momentum shifts. In addition to these effects, when jets are observed at large separations in rapidity, dynamical contributions arise from QCD multi-parton radiation [15–17], calling for perturbative resummations of large-rapidity logarithms to all orders in $\alpha_{\rm s}$. Moreover, with increasing rapidities the nonperturbative parton distributions are probed in highly asymmetric parton kinematics. In particular, jet production becomes sensitive to small-x dynamics in the pdfs. This, in turn, implies that effects from multiple parton collisions [18, 19] become more important [20–22] due to the increase in the parton densities.

First forward jet measurements have been performed by LHC experiments [23, 24]. While inclusive forward jet spectra are roughly in agreement with predictions from different Monte Carlo simulations, detailed aspects of production rates and correlations [23, 24] are not well understood yet.

An example is given by the di-jet observables proposed in [25] associated with events containing a forward and a central jet. Experimental measurements and Monte Carlo comparisons are shown in Fig. 5 [23]. This indicates that none of the Monte Carlo generators describes the data well in all regions, and that, in particular, NLO-matched calculations from POWHEG give large differences in the forward jet p_{T} distribution when combined with different parton showers, see POWHEG+HERWIG *versus* POWHEG+PYTHIA.

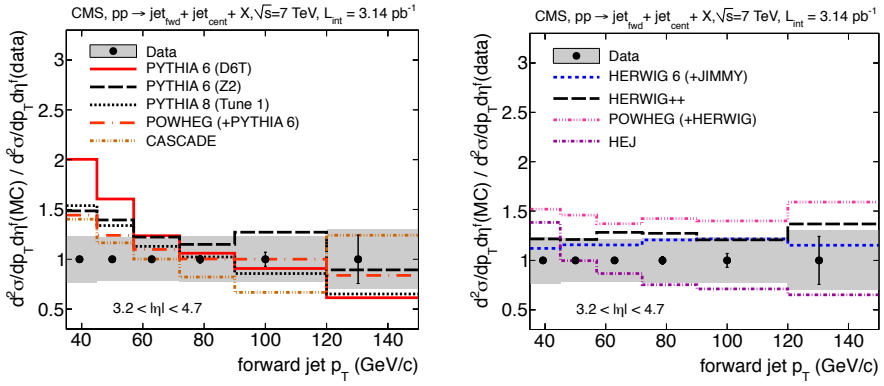

Fig. 5. Ratio theory/data [23] for di-jet events with a central and a forward jet as a function of the forward jet transverse momentum.

In [25, 26], this behavior is investigated by studying the ΔR jet distribution, in azimuth and rapidity space, which quantifies to what extent jets are dominated by hard partons in the matrix element or originate from showering. Large contributions to jets from showering are found [25] in the case of asymmetric parton kinematics, *i.e.* when one of the initial-state showers goes down to small x. Reference [26] furthers this study by considering the central jet transverse energy spectrum, in di-jet events with a central and a forward jet, using the NLO event generator POWHEG matched with parton showers PYTHIA and HERWIG. Figure 6 [26] shows results for the two cases, normalized to the result obtained by switching off parton showering. The marked differences between the two cases are consistent with the findings in [23], and with the large contribution to jets from showering found in [25]. In particular, in the forward–central events considered high-rapidity correlations appear to affect the behavior of jet distributions in the central region.

A classic test of QCD high-energy resummation for jets at large rapidity separations [15] is given by the azimuthal decorrelation between jets. Figure 7 (from [25]) shows the cross section as a function of the azimuthal distance $\Delta\phi$ between central and forward jets reconstructed with the Siscone algorithm [27] ($R = 0.4$), for different rapidity separations. It shows results

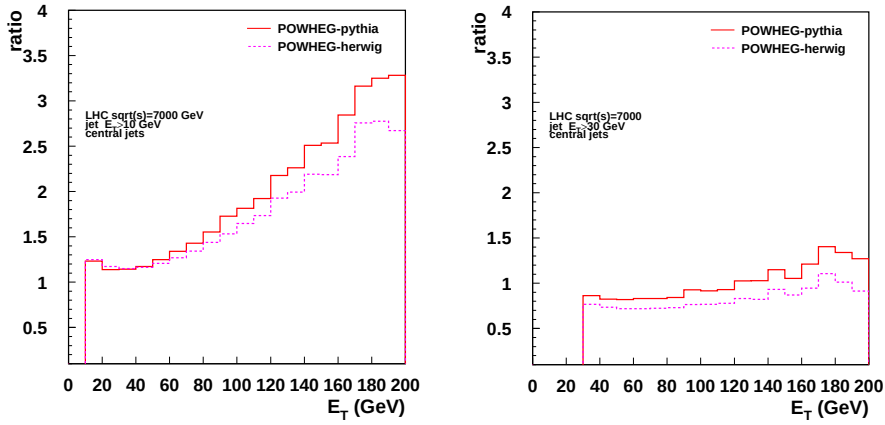

Fig. 6. Ratio of NLO+shower to no-shower results for di-jet events with a central and a forward jet as a function of the central jet transverse momentum [26]. $E_{\mathrm{T}} > 10$ GeV (left); $E_{\mathrm{T}} > 30$ GeV (right).

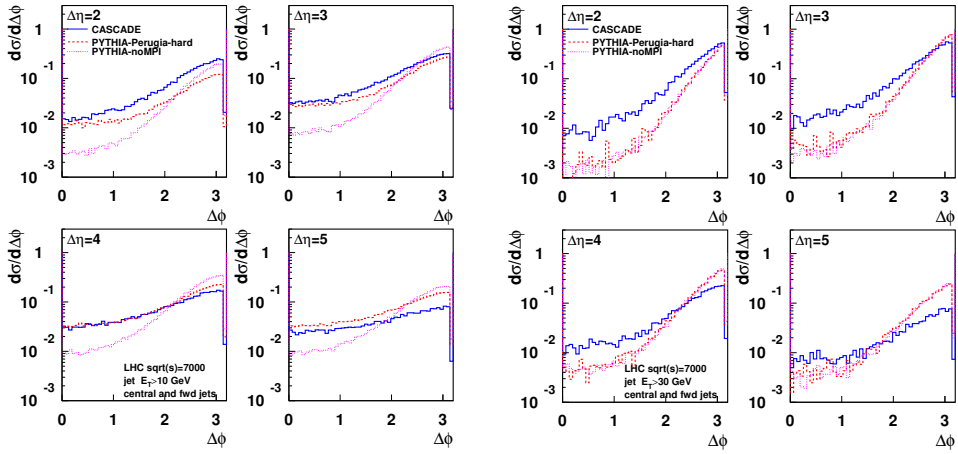

Fig. 7. Cross section *versus* azimuthal distance $\Delta\phi$ between central and forward jet, at different rapidity separations $\Delta\eta$, for jets with transverse energy $E_{\mathrm{T}} > 10$ GeV (left) and $E_{\mathrm{T}} > 30$ GeV (right) [25].

computed by PYTHIA Monte Carlo [28], with and without multi-parton interactions, and by CASCADE Monte Carlo [29], which includes small-x gluon coherence effects [30] in the initial-state shower. The main point is that the decorrelation as a function of $\Delta\eta$ increases in CASCADE as well as in PYTHIA, respectively as a result of finite-angle gluon radiation in single-chain parton shower or as a result of multiple-chain collinear showers; but while in the low E_{T} region (Fig. 7 (left)) this is similar between CASCADE and PYTHIA

with multiparton interactions for $\Delta\eta < 4$, in the higher E_{T} region (Fig. 7 (right)) the influence of multiparton interactions in PYTHIA is small and CASCADE predicts everywhere a larger decorrelation. We will come back to further discussion of correlations in Sec. 5 from the point of view of energy flow observables.

While the specific results shown in this section refer to forward–central jet correlations, it is interesting to consider extensions to the forward–backward kinematics. This will allow one to address the large-Δy di-jet data sets [24], currently rather poorly understood; to search for Mueller–Navelet effects [15]; to analyze backgrounds in Higgs boson studies [31] from vector boson fusion channels. In particular, one may be able to extract information on Higgs properties and couplings from jet kinematics [32]. In this case, too finite-angle radiative contributions to single-chain showers, extending across the whole rapidity range, affect the underlying jet activity accompanying the Higgs [33] and may give competing effects to multiple-parton interactions.

4. *b*-flavor jets

Some of the features observed for inclusive jets in Sec. 2 are also present in *b*-flavor jets [34, 35]. Figure 8 [34] shows a comparison of the measured *b*-jet transverse momentum spectra with matched NLO-shower calculations using MC@NLO [36]. The description of the data is generally good at central rapidities, while at large rapidity and large p_{T} the Monte Carlo is above the data. Similar behavior is shown by comparisons with POWHEG [37] in [35].

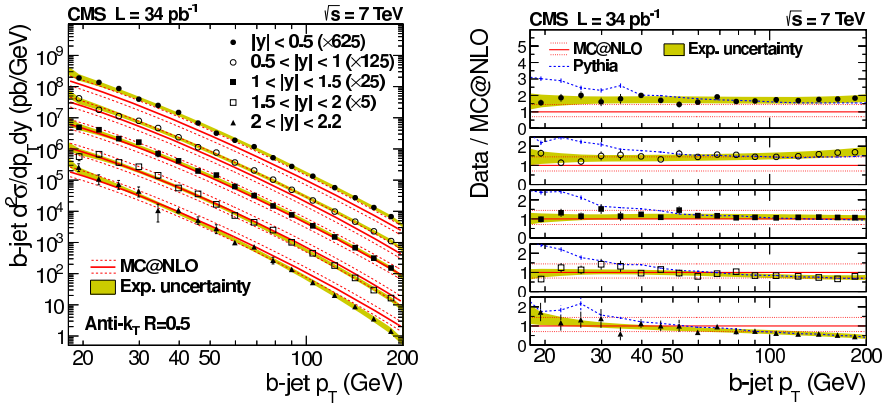

Fig. 8. Inclusive *b*-jet spectra [34].

Figure 9 [9] studies kinematic corrections to *b*-jet production due to longitudinal momentum shifts in the initial state parton shower, similar to those discussed for inclusive jets in Fig. 4. For *b*-jets in different rapidity

regions [34], the gluon x distribution is plotted from POWHEG before parton showering and after including various components of the parton shower generator. The PYTHIA parton shower is used (tune Z2 [38], here including hadronization to identify the b-jet). Figure 9 shows similar shifts in longitudinal momentum with increasing rapidity as in the inclusive jet case. A better understanding of b production in this region is also important for studies of the Higgs to $b\bar{b}$ decay channel, *e.g.* in the associated production with vector bosons.

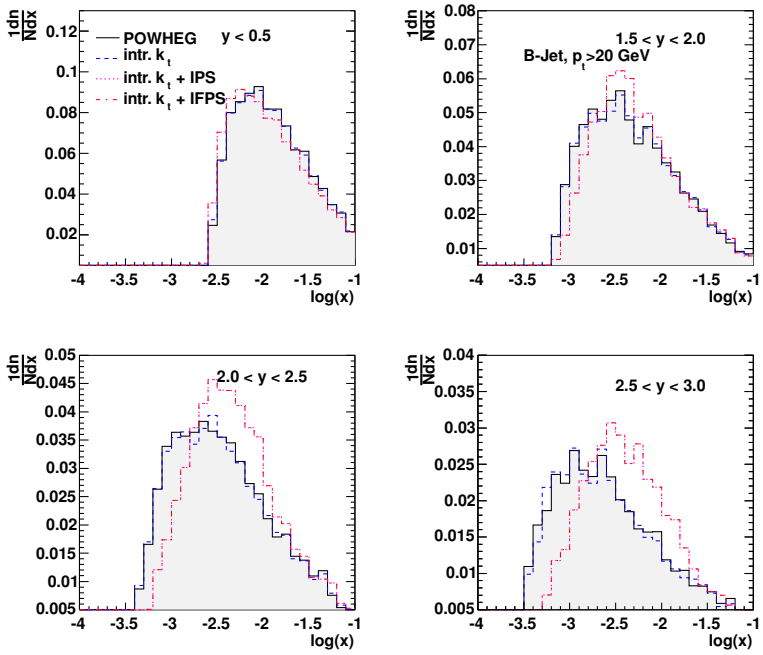

Fig. 9. Production of b-jets: distribution in the parton longitudinal momentum fraction x, before and after parton showering, for different rapidity regions. Shown is the effect of intrinsic k_t, initial (IPS) and initial+final state (IFPS) parton shower [9].

Although for explicit calculations in Fig. 9 a particular NLO-shower matching scheme (POWHEG) is used, the effect is common to any calculation matching NLO with collinear showers. As discussed in [9, 10], the kinematic shifts due to the momentum reshuffling can affect predictions of matched NLO-shower calculations both through the perturbative weight for each event and through the evaluation of the parton distribution functions. In calculations using integrated parton density functions this implies that correction factors as discussed in Sec. 2 have to be applied after the evaluation of the cross section. On the other hand, we note that this is avoided in

approaches using transverse momentum dependent PDFs [39–41] from the beginning (TMDs or uPDFs). It will be of interest to study this quantitatively in Monte Carlo generators which implement these PDFs [42, 43].

5. Multi-parton interactions and energy flow variables

Besides jet cross sections, event shape variables are studied at the LHC [44, 45] and used to characterize the detailed structure of final states and the events' energy flow. First measurements of LHC hadronic event shapes [44] indicate that parton showering effects dominate over contributions from hard matrix elements evaluated at high multiplicity. Jet shape variables describing the jet's internal structure and the energy flow within a jet are also studied [46], and are sensitive, besides jet substructure, to soft dynamics including underlying events [12], pile-up, and multiple parton interactions [20].

Energy flow measurements [47] in minimum bias and di-jet events, designed to investigate properties of the soft underlying event, emphasize the difficulty [48] in achieving a unified underlying event description from central to forward rapidities, based on PYTHIA [28] Monte Carlo tuning. Forward–backward correlations [49] in minimum bias may help analyze the event structure. Complementary to the above measurements are transverse energy flow observables associated with the production of jets widely separated in rapidity [50], sensitive to harder color radiation, and useful for studies of showering and of multi-parton interactions [51]. The transverse energy flow may be defined by summing the energies over all particles in the final states above a minimum E_{T}, or alternatively [50] by first clustering particles into jets by means of a jet algorithm, and then constructing the associated energy flow from jets with transverse energy above a given lower bound q_0. In the latter case, one measures a (mini)jet energy flow, and infrared safety is ensured by the use of the clustering algorithm.

Figures 10 and 11 report results for the particle and minijet energy flow associated with production of central and forward jets [50] from three Monte Carlo event generators: the $k_\perp$-shower CASCADE generator [29], to evaluate contributions of high-energy logarithmic corrections; the NLO matched POWHEG generator [6], to evaluate the effects of NLO corrections to matrix elements; PYTHIA Monte Carlo [28], used in two different modes: with the LHC tune Z1 [38] (PYTHIA-mpi) to evaluate contributions of multi-parton interactions, and without any multi-parton interactions (PYTHIA-nompi).

Figure 10 shows the pseudorapidity dependence of the transverse energy flow in the region between the central and forward jets. The particle energy flow plot on the left in Fig. 10 shows the jet profile picture, and indicates enhancements of the energy flow in the inter-jet region with respect to the PYTHIA-nompi result from higher order emissions in CASCADE and from

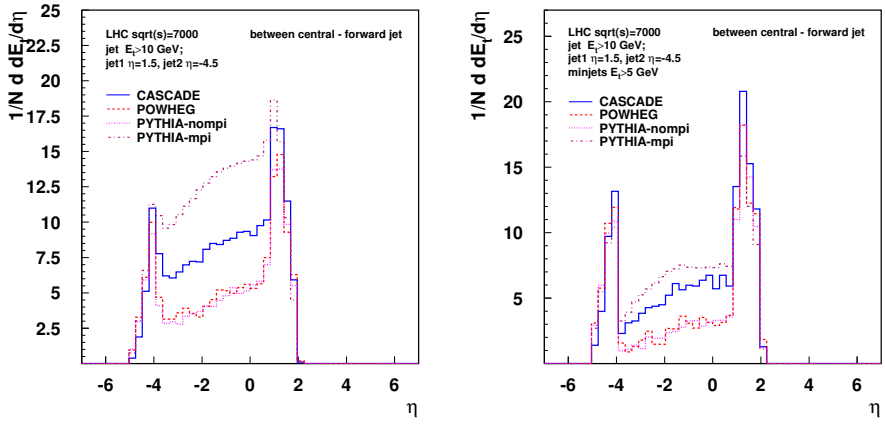

Fig. 10. Transverse energy flow [50] in the inter-jet region: (left) particle flow; (right) mini-jet flow.

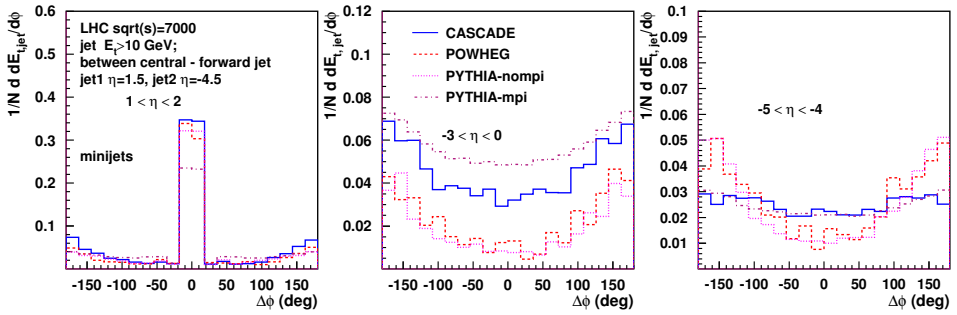

Fig. 11. Azimuthal dependence of the mini-jet energy flow [50] for different rapidity ranges: (left) central-jet; (middle) intermediate; (right) forward-jet.

multiple parton collisions in PYTHIA-mpi. On the other hand, there is little effect from the next-to-leading hard correction in POWHEG with respect to PYTHIA-nompi. The energy flow is dominated by multiple-radiation, parton-shower effects. The mini-jet energy flow plot on the right in Fig. 10 indicates similar effects, with reduced sensitivity to infrared radiation. As the mini-jet flow definition suppresses the contribution of soft radiation, the CASCADE and PYTHIA-mpi results become more similar in the inter-jet region. Distinctive effects are also found in [50] by computations in the region away from the jets.

Figure 11 illustrates the azimuthal dependence of the mini-jet transverse energy flow. Here $\Delta\phi$ is measured with respect to the central jet. The $\Delta\phi$ distribution is shown for three different rapidity ranges, corresponding to the central-jet, forward-jet, and intermediate rapidities. As we go toward

forward rapidity, the CASCADE and PYTHIA-mpi calculations give a more pronounced flattening of the $\Delta\phi$ distribution compared to POWHEG and PYTHIA-nompi, corresponding to increased decorrelation between the jets.

The above numerical results indicate that soft multi-gluon emission over large rapidity intervals gives sizeable contribution to the inter-jet energy flow. As a result, the rates for multi-parton interactions [20] may be influenced significantly by non-collinear corrections to single-chain showering. This also underlines the relevance of approaches which aim at a more accurate and complete description of initial state dynamics by generalizing the notion of parton distributions [39], both for quark-dominated [52] and gluon-dominated [53] processes.

6. Towards low p_{T}

It has been observed in [54] that if jet measurements at the LHC are extended down to transverse momenta of the order of a few GeV one can define a visible leading jet cross section sensitive to the unitarity bound set by the inelastic proton–proton rate which has recently been measured [55–57]. This can be done within the range of acceptance of the measurement without using any extrapolation [54]. Because of the low transverse momenta, this will rely primarily on jets constructed from charged tracks. Given the decay in particle tracking capabilities with increasing rapidity, one may focus on the central pseudorapidity range.

The main interest of these measurements is the possibility to investigate the leading jet cross section near the p_{T} region, $p_{\mathrm{T}} = \mathcal{O}$ (a few GeV), where the inelastic pp production rate is saturated [54]. Even though at weak coupling, dynamical effects slowing down the rise of the cross section in this region involve strong fields and nonperturbative physics. To this end, Ref. [54] introduces an event cross section, defined as an integral over the differential leading jet cross section, which does not depend on the jet multiplicity. Figure 12 shows the visible jet cross section using PYTHIA [8] with jets reconstructed by the anti-k_{T} algorithm [11] for $R = 0.5$ down to low transverse momenta.

In Fig. 12 (left), the perturbative result reaches the inelastic bound [55] for minimum $p_{\mathrm{T}} \simeq 4$ GeV. In the region just above this value, $p_{\mathrm{T}} = \mathcal{O}(10)$ GeV, effects responsible for the taming of the cross section set in. Figure 12 (right) shows the cross section based on the model [19, 58], in which the rise of the cross section is tamed at small values of p_{T} by introducing a p_{T0} cut-off parameter obtained from fits to describe measurements of the underlying event.

Figure 13 [54] shows a comparison of the jet cross section for $p_{\mathrm{T0}} = 0$, including parton shower and hadronisation, with the cross section obtained from PYTHIA including the p_{T0} model. In Fig. 13 (right), we show the effect

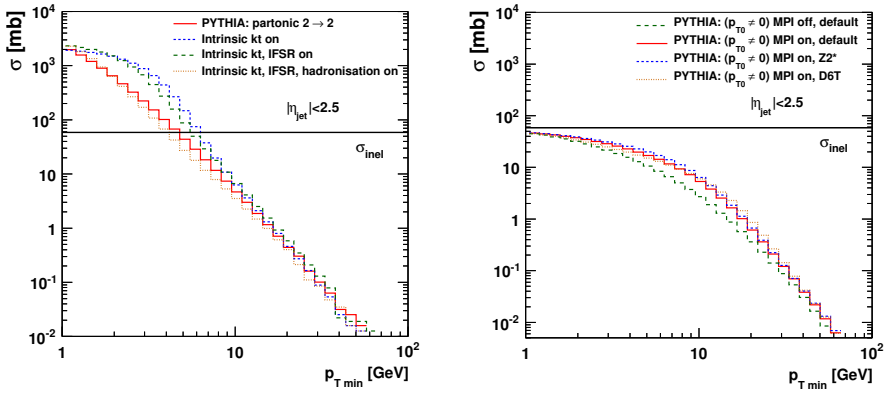

Fig. 12. Left: Cross section from purely partonic $2 \to 2$ process, including intrinsic k_{t}-effects, including initial and final state parton showers (IFSR) and finally hadronisation. Right: predicted cross section applying $p_{\mathrm{T0}} \neq 0$ and MPI with different underlying event tunes of PYTHIA [54].

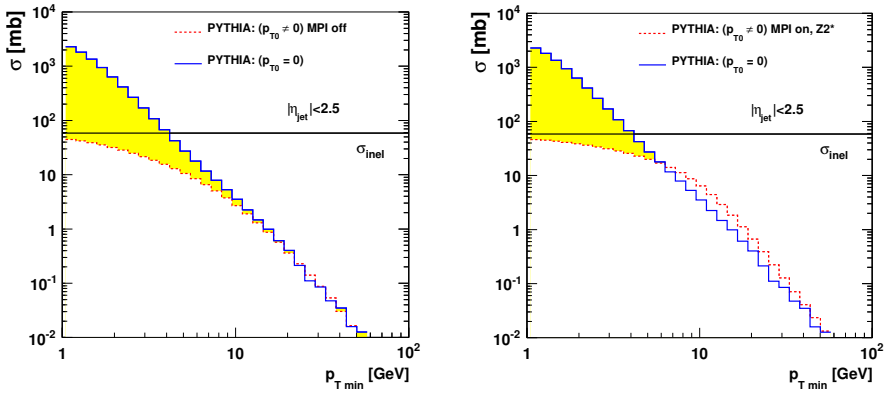

Fig. 13. The cross section as a function of $p_{\mathrm{T\,min}}$ as predicted by PYTHIA in the range $|\eta| < 2.5$. The solid (blue) line shows the prediction applying $p_{\mathrm{T0}} = 0$ including parton shower and hadronisation, while the dashed (red) line shows the prediction with $p_{\mathrm{T0}} \neq 0$; (left) is without multi-parton interactions, (right) including multi-parton interactions with tune Z2* [38].

of multi-parton interactions. Especially in the region of $p_{\mathrm{T}} < 10$ GeV, a clear deviation from the $p_{\mathrm{T0}} = 0$ prediction is visible. Measuring the jet cross section in this range would provide insight into the transition from the large-p_{T} perturbative behavior to the small-p_{T} region where weak-coupling but nonperturbative effects are needed to avoid unitarity violation. The measurement [59] illustrates the feasibility of measuring jets at low p_{T} but it does not examine event cross sections and unitarity effects, while Monte Carlo models are effectively normalized to the lowest p_{T} bin [59].

Besides pp collisions, it is interesting to extend the low p_{T} jet measurements to collisions of nuclei. If the inelastic cross section is measured in AA and pA, they may be useful to characterise properties of final states in terms of jets or flows, and investigate the role of transverse momentum dependent effects and multi-parton interactions [60] in ion collisions.

Many thanks to Wojciech Broniowski, Wojciech Florkowski, Michal Praszalowicz for the kind invitation and warm hospitality at the International Symposium on Multiparticle Dynamics. The material presented in this article originated from discussion and collaboration with many people, in particular, S. Dooling, D. d'Enterria, A. Grebenjuk, P. Gunnellini, M. Deak H. Jung, Z. Nagy, P. Katsas, A. Knutsson, K. Kutak, K. Rabbertz.

REFERENCES

[1] G. Aad *et al.* [ATLAS Coll.], *Phys. Rev.* **D86**, 014022 (2012).

[2] S. Chatrchyan *et al.* [CMS Coll.], *Phys. Rev. Lett.* **107**, 132001 (2011); arXiv:1212.6660 [hep-ex].

[3] K. Rabbertz, review talk at ISMD 2012, Kielce, September 2012.

[4] P. Nason, B.R. Webber, arXiv:1202.1251 [hep-ph].

[5] S. Höche, SLAC preprint SLAC-PUB-14498 (2011); S. Höche, M. Schönherr, *Phys. Rev.* **D86**, 094042 (2012).

[6] S. Alioli *et al.*, *J. High Energy Phys.* **1104**, 081 (2011).

[7] G. Corcella *et al.*, *J. High Energy Phys.* **0101**, 010 (2001) [arXiv:hep-ph/0011363]; G. Corcella *et al.*, arXiv:hep-ph/0210213.

[8] T. Sjöstrand, S. Mrenna, P. Skands, *J. High Energy Phys.* **0605**, 026 (2006).

[9] S. Dooling, P. Gunnellini, F. Hautmann, H. Jung, arXiv:1212.6164 [hep-ph].

[10] F. Hautmann, H. Jung, *Eur. Phys. J.* **C72**, 2254 (2012).

[11] M. Cacciari, G. Salam, G. Soyez, *J. High Energy Phys.* **0804**, 063 (2008).

[12] Z. Ajaltouni *et al.*, arXiv:0903.3861 [hep-ph].

[13] D. d'Enterria, arXiv:0911.1273 [hep-ex].

[14] M. Grothe *et al.*, arXiv:1103.6008 [hep-ph].

[15] A.H. Mueller, H. Navelet, *Nucl. Phys.* **B282**, 727 (1987); C. Ewerz *et al.*, *J. Phys. G* **26**, 696 (2000); S. Catani *et al.*, *Nucl. Phys. B Proc. Suppl.* **29A**, 182 (1992); D. Colferai *et al.*, *J. High Energy Phys.* **1012**, 026 (2010).

[16] S. Catani *et al.*, *Phys. Lett.* **B242**, 97 (1990); *Nucl. Phys.* **B366**, 135 (1991); *Phys. Lett.* **B307**, 147 (1993); *Phys. Lett.* **B315**, 157 (1993); *Nucl. Phys.* **B427**, 475 (1994).

[17] M. Deak, F. Hautmann, H. Jung, K. Kutak, *J. High Energy Phys.* **0909**, 121 (2009); arXiv:0908.1870 [hep-ph].

[18] N. Paver, D. Treleani, *Nuovo Cim.* **A70**, 215 (1982).

[19] T. Sjöstrand, M. van Zijl, *Phys. Rev.* **D36**, 2019 (1987).

[20] P. Bartalini, L. Fanò (eds.), Proc. 1st MPI Workshop (Perugia, 2008), arXiv:1003.4220 [hep-ex]; P. Bartalini *et al.*, arXiv:1111.0469 [hep-ph].

[21] M. Diehl, arXiv:1111.0272 [hep-ph].

[22] Yu.L. Dokshitzer, arXiv:1203.0716 [hep-ph].

[23] S. Chatrchyan *et al.* [CMS Coll.], *J. High Energy Phys.* **1206**, 036 (2012).

[24] G. Aad *et al.* [ATLAS Coll.], *J. High Energy Phys.* **1109**, 053 (2011); S. Chatrchyan *et al.* [CMS Coll.], *Eur. Phys. J.* **C72**, 2216 (2012).

[25] M. Deak *et al.*, arXiv:1012.6037 [hep-ph]; F. Hautmann, *PoS* **ICHEP2010**, 108 (2010); arXiv:1101.2656 [hep-ph].

[26] M. Deak *et al.*, arXiv:1206.7090 [hep-ph].

[27] G.P. Salam, G. Soyez, *J. High Energy Phys.* **0705**, 086 (2007); M. Cacciari, G.P. Salam, G. Soyez, http://fastjet.fr

[28] P. Skands, *Phys. Rev.* **D82**, 074018 (2010).

[29] H. Jung *et al.*, *Eur. Phys. J.* **C70**, 1237 (2010).

[30] M. Ciafaloni, *Nucl. Phys.* **B296**, 49 (1988); S. Catani, F. Fiorani, G. Marchesini, *Nucl. Phys.* **B336**, 18 (1990); G. Marchesini, B.R. Webber, *Nucl. Phys.* **B386**, 215 (1992); F. Hautmann, H. Jung, *J. High Energy Phys.* **0810**, 113 (2008); *AIP Conf. Proc.* **1056**, 79 (2008) [arXiv:0808.0873 [hep-ph]]; arXiv:0804.1746 [hep-ph].

[31] S. Chatrchyan *et al.* [CMS Coll.], *Phys. Lett.* **B713**, 68 (2012); *Phys. Lett.* **B710**, 403 (2012); G. Aad *et al.* [ATLAS Coll.], *Phys. Rev. Lett.* **108**, 111803 (2012); *J. High Energy Phys.* **1209**, 070 (2012).

[32] A. Djouadi, R.M. Godbole, B. Mellado, K. Mohan, arXiv:1301.4965 [hep-ph].

[33] M. Deak *et al.*, arXiv:1006.5401 [hep-ph]; F. Hautmann, H. Jung, V. Pandis, *AIP Conf. Proc.* **1350**, 263 (2011) [arXiv:1011.6157 [hep-ph]]; F. Hautmann, arXiv:0909.1240 [hep-ph]; *Phys. Lett.* **B535**, 159 (2002).

[34] S. Chatrchyan *et al.* [CMS Coll.], *J. High Energy Phys.* **1204**, 084 (2012).

[35] G. Aad *et al.* [ATLAS Coll.], *Eur. Phys. J.* **C71**, 1846 (2011).

[36] S. Frixione, P. Nason, B.R. Webber, *J. High Energy Phys.* **0308**, 007 (2003).

[37] S. Frixione, P. Nason, G. Ridolfi, *J. High Energy Phys.* **0709**, 126 (2007).

[38] R.D. Field, arXiv:1010.3558 [hep-ph].

[39] J.C. Collins, *Foundations of Perturbative QCD*, Cambrigde University Press, 2011.

[40] E. Avsar, arXiv:1203.1916 [hep-ph]; arXiv:1108.1181 [hep-ph].

[41] F. Hautmann, *Acta Phys. Pol. B* **40**, 2139 (2009); *Phys. Lett.* **B655**, 26 (2007); F. Hautmann, H. Jung, *Nucl. Phys. Proc. Suppl.* **184**, 64 (2008) [arXiv:0712.0568 [hep-ph]]; J. Bartels *et al.*, arXiv:0902.0377 [hep-ph]; F. Hautmann, M. Hentschinski, H. Jung, *Nucl. Phys.* **B865**, 54 (2012); arXiv:1205.6358 [hep-ph]; arXiv:1209.6305 [hep-ph].

[42] H. Jung *et al.*, arXiv:1206.1796 [hep-ph].

[43] S. Jadach *et al.*, *Acta Phys. Pol. B* **43**, 2067 (2012); S. Jadach, M. Skrzypek, *Acta Phys. Pol. B* **40**, 2071 (2009).

[44] V. Khachatryan *et al.* [CMS Coll.], *Phys. Lett.* **B699**, 48 (2011).

[45] G. Aad *et al.* [ATLAS Coll.], *Eur. Phys. J.* **C72**, 2211 (2012).

[46] G. Aad *et al.* [ATLAS Coll.], *J. High Energy Phys.* **1205**, 128 (2012); *Phys. Rev.* **D83**, 052003 (2011); S. Chatrchyan *et al.* [CMS Coll.], *J. High Energy Phys.* **1206**, 160 (2012).

[47] S. Chatrchyan *et al.* [CMS Coll.], *J. High Energy Phys.* **1111**, 148 (2011).

[48] P. Bartalini, L. Fanò, arXiv:1103.6201 [hep-ex].

[49] P. Skands, K. Wraight, *Eur. Phys. J.* **C71**, 1628 (2011).

[50] M. Deak, F. Hautmann, H. Jung, K. Kutak, *Eur. Phys. J.* **C72**, 1982 (2012); arXiv:1112.6386 [hep-ph].

[51] F. Hautmann, arXiv:1205.5411 [hep-ph].

[52] M. Garcia-Echevarria, A. Idilbi, I. Scimemi, *J. High Energy Phys.* **1207**, 002 (2012); *Phys. Rev.* **D84**, 011502 (2011); J.-Y. Chiu, A. Jain, D. Neill, I.Z. Rothstein, *J. High Energy Phys.* **1205**, 084 (2012); S. Mert Aybat, T.C. Rogers, *Phys. Rev.* **D83**, 114042 (2011); P.J. Mulders, T.C. Rogers, *Phys. Rev.* **D81**, 094006 (2010); S. Mantry, F. Petriello, *Phys. Rev.* **D84**, 014030 (2011); *Phys. Rev.* **D83**, 053007 (2011); Y. Li, S. Mantry, F. Petriello, *Phys. Rev.* **D84**, 094014 (2011); A. Jain, M. Procura, W.J. Waalewijn, *J. High Energy Phys.* **1204**, 132 (2012); T. Becher, M. Neubert, *Eur. Phys. J.* **C71**, 1665 (2011); I.W. Stewart, F.J. Tackmann, W.J. Waalewijn, *J. High Energy Phys.* **1009**, 005 (2010); F.A. Ceccopieri, *Mod. Phys. Lett.* **A24**, 3025 (2009); I. Cherednikov, N. Stefanis, arXiv:1104.0168 [hep-ph]; *Phys. Rev.* **D80**, 054008 (2009); *Mod. Phys. Lett.* **A24**, 2913 (2009); *Nucl. Phys.* **B802**, 146 (2008); *Phys. Rev.* **D77**, 094001 (2008); J.C. Collins, F. Hautmann, *J. High Energy Phys.* **0103**, 016 (2001); *Phys. Lett.* **B472**, 129 (2000); F. Hautmann, *Nucl. Phys.* **B604**, 391 (2001); arXiv:0708.1319 [hep-ph]; F. Hautmann, *Int. J. Mod. Phys.* **A16S1A**, 238 (2001) [arXiv:hep-ph/0011381]; arXiv:hep-ph/0105098; *AIP Conf. Proc.* **578**, 408 (2000) [arXiv:hep-ph/0101006].

[53] F. Dominguez, J.W. Qiu, B.W. Xiao, F. Yuan, *Phys. Rev.* **D85**, 045003 (2012); F. Dominguez, A.H. Mueller, S. Munier, B.W. Xiao, *Phys. Lett.* **B705**, 106 (2011); F. Dominguez, C. Marquet, B.W. Xiao, F. Yuan, *Phys. Rev.* **D83**, 105005 (2011); B.W. Xiao, F. Yuan, *Phys. Rev.* **D82**, 114009 (2010); *Phys. Rev. Lett.* **105**, 062001 (2010); F. Dominguez, B.W. Xiao, F. Yuan, *Phys. Rev. Lett.* **106**, 022301 (2011) [arXiv:1009.2141 [hep-ph]]; F. Hautmann, D.E. Soper, *Phys. Rev.* **D75**, 074020 (2007); *Phys. Rev.* **D63**,

011501 (2000); F. Hautmann, arXiv:0812.2873 [hep-ph]; *Phys. Lett.* **B643**, 171 (2006); *J. High Energy Phys.* **0210**, 025 (2002) [arXiv:hep-ph/0209320]; *J. High Energy Phys.* **0204**, 036 (2002) [arXiv:hep-ph/0105082]; F. Hautmann, Z. Kunszt, D.E. Soper, *Nucl. Phys.* **B563**, 153 (1999) [arXiv:hep-ph/9906284]; *Phys. Rev. Lett.* **81**, 3333 (1998) [arXiv:hep-ph/9806298].

[54] A. Grebenyuk *et al.*, *Phys. Rev.* **D86**, 117501 (2012).

[55] G. Aad *et al.* [ATLAS Coll.], *Nature Commun.* **2**, 463 (2011).

[56] CMS Collaboration, CMS-PAS-QCD-11-002.

[57] CMS Collaboration, CMS-PAS-FWD-11-001.

[58] T. Sjöstrand, P. Skands, *J. High Energy Phys.* **0403**, 053 (2004).

[59] G. Aad *et al.* [ATLAS Coll.], *Phys. Rev.* **D84**, 054001 (2011).

[60] D. d'Enterria, A.M. Snigirev, *Phys. Lett.* **B718**, 1395 (2013) [arXiv:1211.0197 [hep-ph]].